Chromatography process development aided by a dye-based assay

Greta Jasulaityte[a], Hans J. Johansson[b], Daniel G. Bracewell[a*]

[a] Department of Biochemical Engineering, University College London, Bernard Katz Building, Gordon Street, London WC1E 6BT, United Kingdom

[b] Purolite, Unit D, Llantrisant Business Park, Llantrisant, South Wales CF72 8LF, United Kingdom

* Corresponding author. E-mail address: d.bracewell@ucl.ac.uk, telephone: +44-20-7679-2374; fax: +44-20-7209-0703

Abstract

The lifetime of chromatography resins typically averages between 10-300 cycles for the manufacture of a therapeutic protein. Developing and establishing the robustness of the method for each separation process represents a significant challenge, and is subject to extensive regulatory oversight. Here, we present a novel fluorescence-based assay for residual aggregated proteins to aid the evaluation of the extent of resin regeneration. The versatility of this method was demonstrated by using strong anion and cation exchange agarose resins Praesto Q and SP in conjunction with bovine serum albumin and monoclonal antibody feed materials. The assay entails applying a molecular rotor dye to a sample of free resin, and measuring the fluorescence intensity using a plate reader or visualising under confocal laser scanning microscope to gain a more detailed characterisation. Following five consecutive chromatography cycles, both methods revealed a 10-fold increase in fluorescence intensity along with a proportional reduction in dynamic binding capacity. Furthermore, the use of the assay suggested that fouling was dependent on spatial bead position in the column, bead channel structure, and cleaning conditions. This work presents a simple assay suitable for use in resin lifetime studies to enhance process understanding.

Keywords: Ion-exchange chromatography; Chromatography resin lifetime; Fluorescent dye; Confocal laser scanning microscopy

1. Introduction

A decrease in resin performance can lead to lower dynamic binding capacity, unsatisfactory product yield and purity, resulting in higher production costs or complete lot failures. The deterioration of chromatography resin occurs from accumulation of remaining biological material such as host cell proteins, exposure to harsh buffers, and mechanical compression resulting in a loss of function and performance [1]. Control and maintenance of resin performance is especially important for the repeated manufacture of injectable biological products, where costs and regulatory standards are high [2].

Levels of fouling caused by biological material can be reduced by tangential or dead-end depth filtration prior to column chromatography, in addition to selecting appropriate cleaning and storage procedures for chromatographic operations. It is essential to establish and validate an effective cleaning protocol for these operations during process development, which is generally achieved in several phases. First phase involves screening a large number of cleaning protocols whilst running them in parallel using scale-down high-throughput approach [3,4]. Next phase involves the identification of most effective protocols from the initial phase and testing them at a larger scale before a manufacturing run, or choosing one protocol to validate straight at the manufacturing scale [5,6]. An effective protocol will significantly increase resin lifetime, and reduce the overall production cost.

The deterioration of resin performance can be evaluated by employing a number of analytical techniques to measure critical quality attributes in the eluate such as gel electrophoresis, or by simply

44 measuring the turbidity, and absorbance. The use of standard gel electrophoresis technique has

45 advanced into miniaturized devices (lab-on-a-chip), which can determine the amount of DNA, RNA,

46 and protein [7]. Turbidity measurements taken at 320 nm can be used to analyse the clearance of high

47 molecular weight (HMW) species and host cell impurities [4,8–10], whereas absorbance measurements

48 at 280 nm can indicate the presence of the desired protein in the flow through, elution, and regeneration

49 steps [11]. The amount of host cell DNA and protein detected indicates the effectiveness of the cleaning-

50 in-place (CIP) and by extension the degree of fouling.

51 Alternative techniques for monitoring the extent of fouling rely on more complex analytical set-ups.

52 Fourier transform infrared spectroscopy with attenuated total reflection sensor (ATR-FTIR) can

53 monitor protein contaminant build up and Protein A ligand leaching, as well as predict dynamic binding

54 capacity, which would be highly beneficial for usage *in situ* with small scale columns [12,13]. However,

55 since the ATR technique can accurately measure only a layer of several micrometres, a mechanical bead

56 compressor and a custom container are required, neither of which are compatible with current automated

57 liquid handling systems (LHS).

58 To understand the impact of repeated cycles on a chromatography resin, microscopy-based techniques

59 can be used to produce highly detailed images, providing insight into the extent and location of residual

60 impurities. Scanning and transmission electron microscopes, for example, can reveal morphological

61 changes to the bead surface under poor cleaning conditions [4,14–19]. However, dry samples are a

62 prerequisite for most forms of electron microscopy imaging, which can compromise the bead structure

63 [20]. In contrast, confocal microscopy enables the resin to remain hydrated, eliminating concerns about

64 the impact of drying processes, and thereby facilitating studies on foulant distribution throughout the

65 entire bead with the help of fluorescently tagged proteins (e.g., in Ref. [16,21]).

66 A non-invasive, fluorescence-based technique developed by Pathak and Rathore [22,23] allowed

67 monitoring of fouling in real time using PreDictor™ plates without additional protein tags. The basis

68 of this approach relied on differential amounts of tyrosine and phenylalanine residues in Protein A resin

69 that absorbed at 303 nm, compared to the higher concentrations of tryptophan in foulants, which caused

70 a shift in the absorbance spectra to 340 nm. This method demonstrated the capacity to monitor ligand

71 leaching in addition to foulant accumulation. However, applicability of this technique has yet to be fully

72 established, since testing has been confined to only a single type of resin.

73 In this study, we propose a sensitive and quick fluorescence dye-based method specific to aggregated

74 proteins in the sample that can be used either in conjunction with automated LHS integrated with plate-

75 based measurement of fluorescence or with confocal microscopy. The method employs a commercially

76 available fluorescent dye PROTEOSTAT® that ceases its free rotation around a single bond, and

77 fluoresces upon binding to protein aggregates. The dye provides a much greater sensitivity towards a

78 broader variety of proteins and conditions compared to its early prototype Thioflavin T. It was

79 developed to have minimal fluorescence in the presence of monomers but displays a 20 to 90-fold

80 increase in fluorescence upon binding to cross-β spine structures [24], which are indicative of

81 aggregates [25–27]. This is to our knowledge the first time this dye technology has been used to examine

82 aggregates in separation materials.

2. Materials and methods

83 2. Materials and methods

84

85 2.1. Materials

86 Lipid-free bovine serum albumin (BSA, Fraction V, Millipore Merck) was used in binding studies with

87 Praesto Q 45 µm jetted agarose resin (Purolite, Llantrisant, Wales). IgG1 was kindly provided by

88 Fujifilm Diosynth Biotechnologies, UK, and used with Praesto SP 45 µm jetted agarose resin (Purolite).

89 Chemicals: Tris (Promega), sodium chloride (Merck Chemicals), sodium acetate and sodium hydroxide

90 (VWR Chemicals), sodium citrate dihydrate and citric acid (Sigma-Aldrich) were used in fouling

91 studies. Proteostat dye (Enzo Life Sciences, Exeter, England) was obtained to measure and visualise

92 fouling with a fluorescence reader and confocal laser scanning microscopy (CLSM).

93 2.2. Controls for the dye assay

94 A number of controls including fresh resin sample, fresh resin with bound BSA, IgG1, and heat-

95 denatured BSA were prepared in addition to the ones provided by the manufacturer: aggregated and

96 lyophilised native lysozyme proteins as well as 1x assay buffer. Heat-denatured BSA sample was

97 prepared by heating the protein at 65 ºC for 35 min to form soluble aggregates [26]. Fresh resin with

98 bound heat-denatured BSA and fresh BSA (both at 10 mg/mL concentration) or IgG1 samples were

99 prepared using a miniature flow cell designed as described in [16] using conditions outlined in Table 1.

100 The flow cell was packed with 50 % Praesto Q or SP slurry (total chamber volume 0.02 mL), washed

101 with deionised water, equilibrated with Tris or sodium citrate buffer, loaded with 30 mg of BSA or 6

102 mg of IgG1, respectively, and then washed again with the equilibration buffer to remove unbound

103 protein. Treated resin was collected to be investigated with the dye.

104 Prior to these experiments, the amount of protein required to completely saturate the beads in a flow

105 cell had to be determined. Therefore, fluorescent Texas Red® labelled BSA was purchased

106 (Invitrogen™), mixed with fresh BSA in a 1:100 ratio [28], and 10 mg/mL of the mixture was loaded

107 onto the flow cell. BSA adsorption was visualised in real time under Leica TCS SPE inverted confocal

108 laser scanning microscopy (Leica Microsystems) for up to 60 min. After 30 min of loading, which

109 equated to 30 mg of material, beads showed complete core saturation. CLSM settings were the same as

110 described in [16].

111 2.3. Fouling studies using different cleaning reagents

112 Dynamic binding capacity (DBC) studies were performed on ÄKTA™ Pure 150 using Tricorn™ 5/50
113 columns (both GE Healthcare, Uppsala, Sweden) packed according to the manufacturer's instructions.
114 Bed height was kept at 5±0.2 cm, packing quality was determined using 5 % acetone and maintained at
115 4675±301 (1SD) plates per meter and 1.44±0.06 (1SD) asymmetry. Fouling study was performed using
116 three flow rates: 125 cm/h (4 consecutive runs) followed by 50 cm/h (3 runs) and 37.5 cm/h (3 runs).
117 200 mg of BSA was loaded per cycle, with conditions used as detailed in Table 1. Samples were taken
118 from the upper part of the column to be investigated with the dye (Figure 1).

119 2.4. Dye sensitivity through an increasing number of cycles

120 Another fouling study was performed in a similar manner as described in the previous section. Here,
121 for simplicity purposes only one flow rate of 50 cm/h was chosen. The runs consisted of equilibration
122 buffer 50 mM Tris, pH 8.5, elution buffer 50 mM Tris, 1.5 M NaCl, pH 8.5, and CIP buffer 1 M NaOH
123 with a hold for 30 min. CIP was carried out after every cycle in an upwards column position. In addition,
124 a monoclonal antibody was used to evaluate the sensitivity of the dye after 25 cycles with a load of up
125 to 1 mg of IgG1 per cycle (condition **e**), Table 1).

126 2.5. Sample preparation for imaging

127 Sample preparation and staining were carried out as detailed in the Proteostat product manual in Costar
128 96-well black, clear bottom polystyrene plates (Fisher Scientific). Each well contained 98 µL of 20 %
129 resin slurry sample in water, and 2 µL of Proteostat dye; plates were incubated in the dark for a
130 minimum of 20 min.

131 2.6. Fluorescence intensity measurement

132 Fluorescence intensity was measured using Tecan Safire[2]™ system (Tecan) with 30 seconds of orbital
133 shaking prior to excitation at 550 nm wavelength, and emission at 600 nm wavelength. Samples were
134 prepared in triplicate.

135 2.7. Fluorescence visualisation

136 Leica TCS SPE inverted confocal microscopy (Leica Microsystems) was used to visualise particular
137 areas of fluorescence (aggregation) in resin samples. Microscopy settings were the same throughout all
138 experiments: magnification 40x with oil immersion, gain 900, intensity 40 %, pinhole 2, excitation
139 wavelength 550-600 nm, and emission wavelength 600 nm. The usual flat or round bottom microscope
140 slides failed to provide good quality images. Therefore, the flow cell was used to contain and provide
141 hydrated environment for resin during imaging (other designs such as 96-well plates could be used with
142 compatible microscopes). At least three images of each sample were taken, but only the most
143 representative ones are shown in this paper.

3. Results and discussion

3.1. Assay development

3.1.1. Dye interacts with the native proteins

Proteostat dye, to our knowledge, has not been combined with chromatography resins or indeed any separation materials, and therefore required a number of controls to be evaluated to ensure resin-dye or monomer-dye interactions would not interfere with the assay. Initial negative controls included fresh resin, fresh BSA and IgG1, bound BSA and IgG1, in addition to positive controls of fresh and bound heat-denatured BSA. Fresh agarose media Praesto Q and SP were shown to lack interactions with the dye leading to basal levels of fluorescence as expected (Fig. 2**i**). In contrast, despite possessing an all α-helix structure [29], bound BSA interacted with the dye producing a fluorescent ring pattern (Fig. 2**iii** and 3**B**). Similarly, outer ring patterns were visible for the bound IgG1 control, although more beads displayed fluorescence throughout the core (Fig. 2**vi**). Fluorescence readings for bound BSA and IgG1 were 5 to 6-fold higher than those for the proteins alone (Fig. 3**B**).

BSA is known to form dimers, trimers, and other oligomers, which are often seen in commercial BSA solutions when analysed on a size exclusion chromatography column [30]. These protein conformations can cause the dye to bind as it has an affinity for β-sheets that are present in dimers. A recent study with an early prototype Thioflavin T revealed that the dye exhibits a 6-fold higher affinity towards BSA dimers than monomers [31]. Conversely, there is also evidence to suggest that the dye can bind to specific parts of monomers, non-β-sheet cavities [32–34], and therefore fails to distinguish between different protein conformations [35].

In order to understand which mechanism prevails in this work, several different approaches were undertaken. Firstly, BSA solution and IgG1 were loaded onto a size exclusion column, whereby chromatograms displayed 10 % and 7 % of HMW species, respectively (results not shown). Fluorescence results indicated that the dye interacted with 18 % and 15 % native BSA and IgG1 when compared to the resin bound proteins (Fig. 3**B**). This supports the previous theory that the Proteostat dye can also interact with a small percentage of monomers in addition to higher oligomers. However, the presence of such interactions is not sufficient to explain the ring pattern seen for both BSA and IgG1 (Fig. 2**iii**, **vi**), and high fluorescence readings (Fig. 3**B**).

Next, we wanted to ensure that the ring pattern was not a result of incomplete bead saturation via an implementation of another dye. Texas Red labelled BSA was loaded onto the miniature flow cell column using the same feed and time conditions as the Proteostat dye experiments. Real-time confocal microscopy confirmed a complete bead core saturation with Texas Red labelled BSA after 30 min (Fig. 2**v**) rejecting the 'incomplete bead saturation' hypothesis, and suggesting species other than intact

178   monomers were the cause origin of the ring structure. Another logical reason for ring formation has
179   been suggested to be large protein size and small resin pores [36]. However, here appropriate resin pore
180   size was selected, and live protein uptake as well as static binding results confirmed much higher levels
181   of protein absorption than in the previous study [36].

182   It is possible to attribute native protein-dye interaction to partial protein unfolding and/or aggregation
183   upon binding to ligands, since the fluorescence readings were significantly higher than those for both
184   non-bound protein solutions (Fig. 3**B**). Whilst BSA has been shown to exhibit this behaviour only at
185   low pH's of 3.0 to 4.5 [37], there has been substantial evidence to support such ligand interactions with
186   antibodies [38–43]. Process conditions such as pH and salt were found to lead to on-column protein
187   unfolding and aggregation. Such factors may be applicable to the IgG1 used in this study (Fig. 2**vi**),
188   since this particular antibody contains high levels of charge variants. Changes to protein conformation
189   upon binding may be enough to partially block resin pores impairing further protein uptake, thus
190   creating rings of accumulated protein. Alternatively, charge-based structural changes may induce
191   stronger or even irreversible binding to resin. Therefore, our working hypothesis is that the Proteostat
192   dye interaction with bound native BSA and IgG1 can be explained as both presence of dimers and
193   conformational changes to the protein structure upon adsorption.

194   3.1.2. Heat-denatured protein blocks bead channels

195   Heat-denatured BSA and Proteostat dye interaction was anticipated as thermal stress above 65 $^{\circ}$C
196   causes a decrease in α-helices while increasing β-sheet formation, resulting in aggregation [44]. This
197   sample revealed an alternate fluorescence profile, whereby protein is primarily distributed on the
198   surface of the bead with round, aggregate-like structures (Fig. 2**ii**) instead of thick rings observed for
199   native BSA (Fig. 2**iii**). These aggregate-like structures may have occluded the resin pores preventing
200   further protein uptake, as observed by limited permeation of the dye. Similar structures, primarily
201   deposited on the resin surface with protruding protein aggregates and interacting with other beads, have
202   also been visualised with scanning electron microscopy [4,16,45]. Additionally, measurement of
203   fluorescence in a plate demonstrated approximately 4-fold higher levels of fluorescence when using
204   heat-denatured instead of native BSA solution, which was comparable to the manufacturer's positive
205   (aggregated lysozyme) control (Fig. 3**B**). In contrast, the fluorescence intensity for the bound protein
206   was 1.4-fold lower than for the non-bound protein solution. This was possibly a result of heat-denatured
207   protein not being able to move through to the core of the bead and eluting prematurely, as aggregate-
208   like structures blocked the entrance (Fig. 2**ii**).

209   3.1.3. Dye has high affinity to deliberately fouled resins

210   Having demonstrated sufficient sensitivity and selectivity from the initial controls, fouled resin samples
211   were prepared. 1 mL columns were packed, and 10 cycles of BSA and 25 cycles of IgG1 were run with
212   loadings of 200 mg and 1 mg per cycle, respectively. Equilibration was performed with 50 mM Tris at

213 pH 8.5, and BSA was eluted with 50 mM Tris, 1.5 M NaCl at pH 4.7 over 15 column volumes (CV)

214 followed by a CIP cycle with 10 CV of 1 M NaOH. Equilibration buffer for the IgG1 runs was 10 mM

215 sodium citrate at pH 5, and elution buffer had additional 0.5 M of NaCl. CIP was not performed for the

216 IgG1 cycles as the elution step seemed to sufficiently remove small amounts of bound protein.

217 Following the runs, the columns were unpacked and the fluorescence intensity was measured by

218 applying the dye onto the samples. Confocal microscopy images revealed that both residual BSA and

219 IgG1 molecules occupied resin following the elution step, and in case of BSA, after the CIP also (Fig.

220 2**iv** and 2**vii**). The residual proteins occupied the entire bead with no particular patterns. We then

221 decided to test whether different cleaning conditions could reduce the amount of residual protein.

222 3.2. Assay utilization to understand fouling

223 3.2.1. Strip and CIP steps are crucial in resin regeneration

224 In order to further evaluate the selectivity of the dye as well as to understand what causes fouling, effects

225 of different cleaning solutions were investigated (Table 1). The routine cleaning procedure for an ion

226 exchange resin uses a high salt concentration strip buffer followed by 1 M sodium hydroxide solution,

227 and therefore variations of this method were selected. Consecutive DBC runs were performed using

228 three different flow rates (125 cm/h for the first 4 consecutive runs, 50 cm/h for the next 3 runs, and

229 37.5 cm/h for the final 3 runs) followed by a particular cleaning regime after every cycle (see Table 1).

230 Total ten cycles with 200 mg loading each were performed for all buffer conditions.

231 After ten DBC runs with fresh BSA, the upper resin fraction in the column (1.7 cm) was collected and

232 the degree of fouling quantified by fluorescence using a plate reader before visualisation under confocal

233 microscopy. Both techniques revealed that using a cleaning regime consisting exclusively of 1 M NaOH

234 (without a strip step) would result in the highest level of fluorescence up to 29,000 RFU indicating the

235 highest degree of fouling compared to other conditions of 6,000 RFU (Fig. 3**B** and 3**C**). This was also

236 in agreement with a 5-fold reduction in DBC at 10% breakthrough for 1 M NaOH condition after 10

237 cycles (Fig. 3**A**). The maximum DBC at 10% breakthrough was found to be around 60 mg/mL, 95

238 mg/mL and 98 mg/mL for 2.4 min, 6 min and 8 min residence time, respectively. Therefore,a strip step

239 was shown to be crucial for column CIP, whereas a sodium hydroxide step alone was insufficient, and

240 led to a dramatic loss in binding capacity. These results support previous findings, whereby both NaOH

241 and NaCl were required to provide appropriate clearance of host cell impurities [21,46].

242 Quantitative fluorescence measurements indicated no significant differences amongst the three salt

243 buffer conditions (Fig. 3**B**), whereas confocal microscopy revealed variation in fluorescence amongst

244 individual beads (Fig. 3**C**). This is particularly visible in images (**iv**) and (**v**), where a single sample was

245 imaged under different laser intensities: 40 and 20 per cent, respectively. High levels of protein

246 aggregation caused by a 1 M NaOH clean were expected to affect more or less all beads equally;

247 however, numerous beads exhibited very low levels of fluorescence at 20 % laser intensity (Fig. 3**C**,

248 image (**v**). We hypothesized that this could be a result of the sampling of a mixed population of beads

249 from the column, which would contain populations from both axial and radial dimensions within the

250 column.

251 3.2.2. Fouling heterogeneity is present at column level

252 Data from initial fouling experiments revealed a non-uniform fluorescence pattern amongst the beads

253 requiring further studies to identify the cause of these variations. It is hypothesised that this variation

254 may be influenced by bead position in the column [18,19]. Logically the upper part of the column,

255 which is subject to exposure to the highest protein loading, would contain the most extensive levels of

256 residual aggregated protein when compared to the lower part of the column. Consequently, the columns

257 were dissected into five parts: top filter, top, middle, bottom, and bottom filter, following DBC runs

258 with one cleaning regime (15 CV gradient strip with 50 mM Tris, 1.5 M NaCl at pH 8.5, and 10 CV

259 CIP with 1 M NaOH plus 30 min hold). Additional IgG1 fouling runs were then performed as described

260 in the 2.4. Methods section. Briefly, 1 mg of IgG1 was loaded for each cycle followed by a 30 CV

261 gradient elution with 10 mM citrate, 0.5 M NaCl, pH 5, and no CIP.

262 The amount of residual aggregated protein increased with cycle number as seen from a decline in

263 binding capacity and increase in fluorescence intensity (Fig. 4). The chosen experimental flow rate (50

264 cm/h), which was equal to 6 minutes of residence time, and high BSA load (200 mg) provided maximum

265 bead saturation resulting in severe levels of fouling. As a result of long residence time resin binding

266 capacity dropped from 100 g/L to a mere 10 g/L only after five binding cycles (Fig. 4A, line graph).

267 Whilst this was not representative of a typical number of chromatography cycles, the dye was sensitive

268 enough to differentiate between severe fouling conditions, and thus would be suitable for less

269 pronounced cases. In contrast, experiments run at a higher flow rate of 125 cm/h (providing 2.4 minutes

270 of residence time) resulted in no decrease in DBC, and undetectable fluorescence under confocal

271 microscopy after 15 cycles (results not shown). Consequently, due to time constraints, the latter

272 experimental conditions were discontinued, and the more extreme fouling case was studied as a proof

273 of concept.

274 Fouling was found to begin in the upper part of the column and continue through to the lower part as

275 the number of cycles increased (Fig. 4). The most upper part of the column exhibited highest

276 fluorescence intensity of 900 RFU during the first cycle followed by a gradual increase in fluorescence

277 for up to 7,900 RFU over the following 2-4 cycles. It culminated with lowest filter section being still

278 reasonably foulant-free after the final 5th cycle with only 5,000 RFU (Fig. 4**A**). Fluorescence data from

279 plate reader measurements and confocal microscopy were concordant with the overall DBC

280 calculations, whereby reduction in capacity was representative of the residual protein accumulation in

281 the upper parts of the column.

282   The fouling pattern seen for the IgG1 cycles is similar to that seen in the BSA example. The aggregate

283   concentration was similar throughout the different parts of the column, where the overall fluorescence

284   intensity was reasonably low and comparable to that of BSA after 2 cycles (Fig. 4). The fluorescence

285   may have been reduced or eliminated if additional CIP cycles had been performed, which has been

286   shown to improve resin recovery [21]. Furthermore, there was a clear sample heterogeneity that can be

287   attributed to the spatial bead location and flow properties in that particular sample [16,17,19]. The

288   hypothesis that small resin beads were fouled first was rejected because the fluorescence was

289   comparable for larger resin beads (Fig. 4**B**). In addition, residual protein was distributed throughout the

290   entire column length, which can be expected due to a high number of cycles. Nevertheless, no particular

291   areas were found to be affected by round aggregate formation apart from the evidence of bead-to-bead

292   contact once the laser intensity was reduced to 20 % for IgG1 samples, whereas 'spotting' patterns

293   could be seen after 2 cycles throughout the whole column and at the bottom filter after 4 and 5 cycles

294   for BSA containing samples (Fig. 4**B**). Such behaviour is likely to indicate that sodium hydroxide

295   causes BSA proteins to form lumps, which are then likely to obstruct smaller pores.

296   3.2.3. Fouling heterogeneity is present at bead level

297   Whilst the dye assay demonstrated an application for resin lifetime studies, it has also revealed a high

298   sensitivity towards spatial foulant distribution patterns at a bead level. Protein deposits after cleaning

299   were identified in different parts of the bead: surface (Fig. 5**i**, **ii**), core (Fig. 5**iii**), and intraparticle voids

300   (Fig. 5**iv**, **v**).

301   Two particular foulant arrangements were identified on bead surfaces using the dye assay (Fig. 5**i**, **ii**).

302   Firstly, foulants were primarily deposited on the surface of the beads forming large interacting

303   structures, which caused pore blockage and reduced the rate of protein uptake (Fig. 5**i**), an observation

304   which has been seen in other reports [16–19,47,48]. Moreover, fluorescence patterns were comparable

305   to the heat-denatured BSA control (Fig. 2**ii**) further supporting the dye's selectivity for the aggregates.

306   Secondly, gaps in bead surface fluorescence were detected (Fig. 5**ii**), which were indicative of particle-

307   particle contact in a packed column resulting in uneven protein uptake [16,17,46,49]. Residual surface

308   protein build-up was shown to be dependent on the spatial hierarchy in the column and proximity to

309   other beads.

310   An overlay of CLSM and transmitted light displayed a fluorescent bead core and a 'halo' surface lining

311   (Fig. 5**iii**). Residual aggregated proteins may have primarily collected in the core rather than the surface,

312   which was much more accessible to the flow of cleaning reagents [19]. Providing chromatography

313   columns are saturated to >70 % instead of 100 % as in this study, the effect to the core may not be as

314   significant. This is especially true for biologics capture steps using Protein A resin at high linear velocity

315   and short residence time, as proteins may not have sufficient time to utilise the full volume of the bead

316   [50,51]. Otherwise, consecutive rounds of hold-wash cycles using 1 M NaOH could provide a more

317 effective clean that would allow to reach the centre of the bead once each layer of residual protein had
318 been washed.

319 Another area of significant aggregate deposition was observed inside and around the intraparticle voids
320 (Fig. 5**iv**, **v**). These voids were detected by transmitted light and confocal microscopy, and previously
321 by both transmission and electron microscopy [14,15], and X-ray computed tomography [52]. Whilst
322 the intraparticle voids did not facilitate protein uptake during the loading step (Fig. 5**vi**), they had
323 distinct affinity towards the fluorescent dye suggesting high aggregate presence (Fig. 5**iv** and 5**v**).
324 Despite having minimal role in protein uptake, the voids proved to be highly fluorescent during the
325 elution step as discussed by Angelo et al. [15]. It was hypothesized that particularly low ligand density
326 in the voids and surrounding narrow channels played a role in both binding and elution steps. We
327 support this hypothesis, as such large empty spaces can act as isolated entities by either having very
328 few or no connections to other channels. Consequently, the flow to and from the voids would be limited
329 leading to uneven or poor diffusion resulting in increased amount of foulant build up. Although voids
330 on the surface of the bead were more accessible to the flow, cleaning reagents were ineffective for both
331 types of voids: present inside and outside of the beads (Fig. 5**iv** and 5**v**).

332 These results demonstrate that contrary to prevailing understanding [14,15], voids can play a significant
333 role in a chromatography process. Such intraparticle structures often form during the bead
334 emulsification process, and is a result of oil-in-water-in-oil double emulsions [53]. Agarose droplets
335 (water phase) are formed with the help of surfactants (oil phase), which can get trapped inside the
336 agarose droplets causing the appearance of intraparticle inclusions. An increase in intraparticle
337 inclusion formation could alter the effective protein binding area resulting in reduced dynamic binding
338 capacity. In addition, the inclusions could lead to an increase in residual protein accumulation, as it
339 could not be removed using traditional cleaning reagents due to spatial channel constraints. Similar
340 hypotheses have been presented [47,48], whereby small intraparticle granules were thought to hinder
341 access to other channels and ligands. Nevertheless, the process of intraparticle void formation can be
342 controlled by reducing the stirrer speed and slowing down agarose addition into the oil phase [54,55].
343 The introduced changes could potentially eliminate this type of fouling phenomenon.

344 ## 4. Concluding remarks
345

346 With the aid of the Proteostat dye, we unveiled a number of different fouling patterns. Firstly, fouling
347 was found to be non-uniform across the entire column length, whereby the upper part of the column
348 was most affected as it was in constant contact with the load material. Secondly, there were differences
349 across the bead populations in specific radial sections, possibly due to variation in liquid flow and access
350 to the bead. Thirdly, the extent of fouling was influenced by the bead structure: pore accessibility and
351 presence of voids. Possession of multiple voids and dead-end channels resulted in higher amount of

residual protein because of obstructed protein and liquid accessibility and manoeuvrability. Furthermore, the assay provided evidence to support the concept of changes in protein conformation due to protein-ligand interaction, as the outer bead areas were particularly fluorescent. Finally, it has been shown visually that different cleaning reagents have different modes of interaction with the bound protein proving that a salt strip is key in the resin regeneration process.

The aggregate detection assay for chromatography resins demonstrated sensitivity, selectivity and robustness for both feed materials BSA and IgG1, and for different types of resin. The dye was able to distinguish between different cleaning regimes, number of cycles, and identify particular areas in the beads prone to fouling. Using a combination of a fluorescence plate reader and confocal microscopy, facilitated the identification of aggregation, and provided support for the dynamic binding capacity results. Based on the reduction in binding capacity and equivalent increase in total fluorescence, we estimate that acceptable fluorescence levels would be up to 20,000 RFU, which would provide up to 60 mg/mL DBC. Sensitivity of the assay plateaus with increasing levels of fouling as it reaches >30,000 RFU (<40 mg/mL DBC). The assay could be further improved with the implementation of a high-throughput liquid handling robot to permit the accurate and rapid screening of multiple samples.
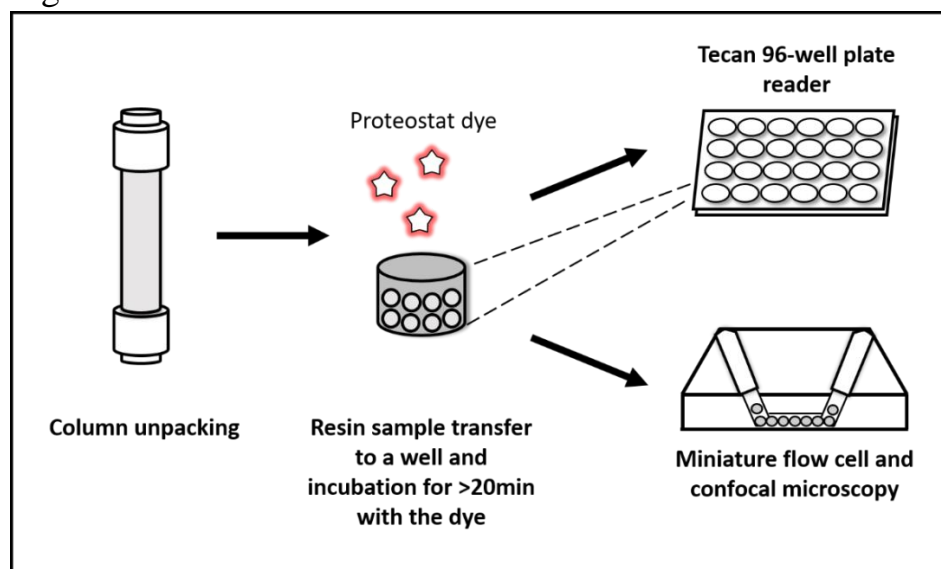
Acknowledgements

371 *Table 1. Small scale chromatography conditions*

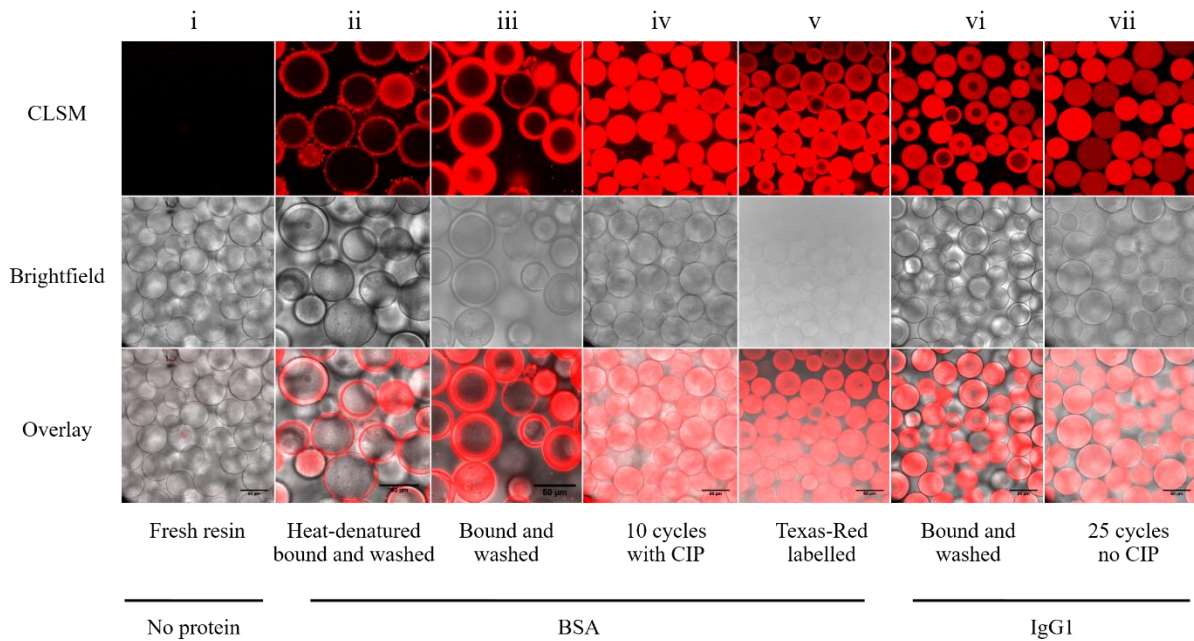| Condition	Feed material	Equilibration and wash	Gradient elution (5 CV)	Strip (100%B, 15 CV)	CIP
a)	Pure BSA	50 mM Tris, pH 8.5	+ 1.5 M NaCl, pH 4.7	Yes	1 M NaOH (30 min hold)
b)	Pure BSA	50 mM Tris, pH 8.5	+ 1.5 M NaCl, pH 4.7	Yes	No
c)	Pure BSA	50 mM Tris, pH 8.5	+ 1.5 M NaCl, pH 4.7	No	1 M NaOH (30 min hold)
d)	Pure BSA	50 mM Tris, pH 8.5	+ 1.5 M NaCl, pH 8.5	Yes	No
e)	IgG1 after Protein A	10 mM sodium citrate, pH 5	+ 0.5 M NaCl, pH 5	Yes	No

372

373 Figures

374

375 *Figure 1. Proteostat dye assay.*

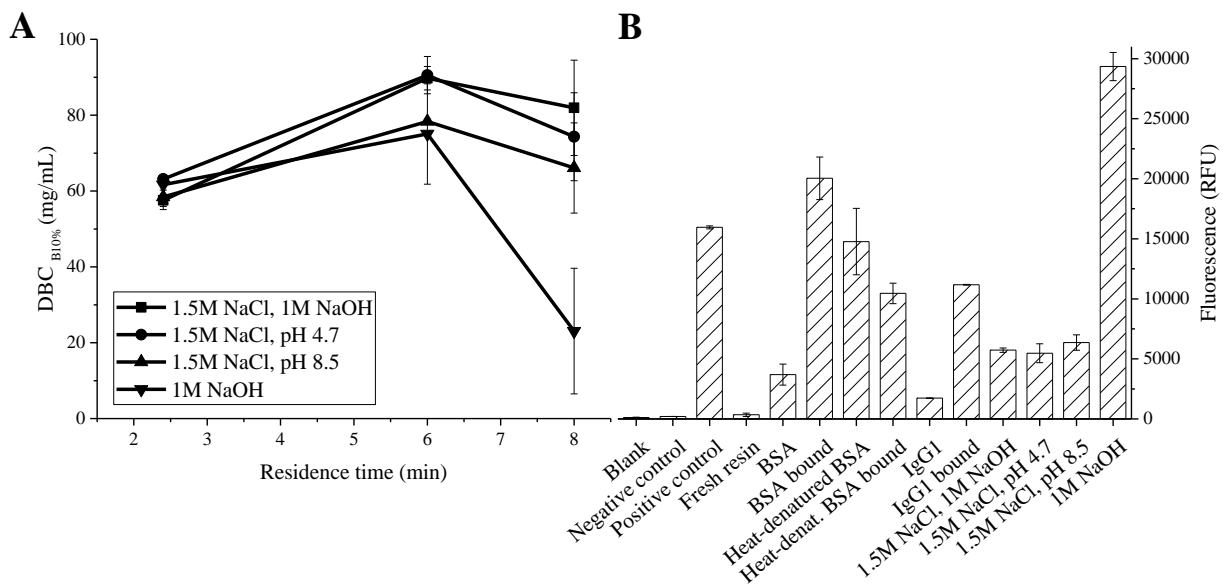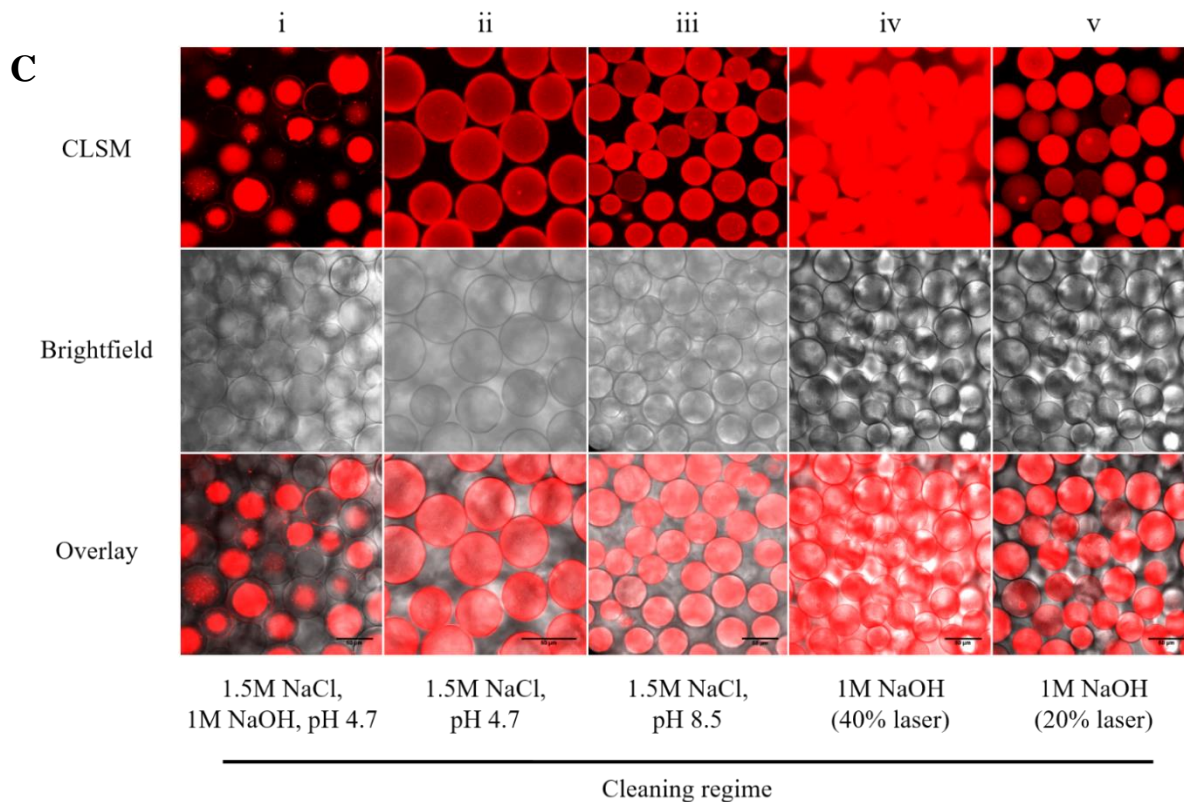|	i	ii	iii	iv	v	vi	vii
CLSM							
Brightfield							
Overlay							
	Fresh resin	Heat-denatured bound and washed	Bound and washed	10 cycles with CIP	Texas-Red labelled	Bound and washed	25 cycles no CIP
	No protein	BSA				IgG1	

376

*Figure 2. Controls for the dye assay. CLSM images of fluorescence, transmitted light, and their overlay are presented. At least three images were taken, and one representative example is shown. Laser intensity was 40 %, excitation was 550 nm and emission was 600 nm for all samples. Images (**ii**) and (**iii**) show a smaller section of a larger image for a clearer representation. Samples for images (**ii**), (**iii**) and (**iv**) were obtained using the Proteostat dye, whereas sample (**v**) was imaged live using Texas Red labelled BSA. Heat-denatured sample (**ii**) was produced after heating BSA at 65 $^{\circ}C$ for 35 min. Equilibration buffer used for samples (**iii**), (**iv**) and (**v**) was 50 mM Tris at pH 8.5, and elution buffer for sample (**iv**) contained additional 1.5 M NaCl followed by a 1 M NaOH clean. Similarly, equilibration buffer for samples (**vi**) and (**vii**) was 10 mM sodium citrate at pH 5, and elution buffer for sample (**vii**) contained 0.5 M NaCl and no CIP.*

387

388

|	i	ii	iii	iv	v
CLSM					
Brightfield					
Overlay					
	1.5M NaCl, 1M NaOH, pH 4.7	1.5M NaCl, pH 4.7	1.5M NaCl, pH 8.5	1M NaOH (40% laser)	1M NaOH (20% laser)

Cleaning regime

*Figure 3. Fouling with different cleaning conditions. **A.** Dynamic binding capacity of 10 cycles using 200 mg of pure BSA at different flow rates (125, 50 and 37.5 cm/h representing 2.4, 6 and 8 minutes of residence time). Four cleaning regimes were chosen: (1) strip with 1.5 M NaCl at buffer pH 4.7 followed by 1 M NaOH CIP, (2) strip with 1.5 M NaCl at buffer pH 4.7, no CIP, (3) strip with 1.5 M NaCl at buffer pH 8.5, with no CIP, (4) no strip, only 1 M NaOH CIP (Table 1). Averages and 1SD were calculated for 4, 3 and 3 consecutive runs. **B.** Fluorescence measurements using Tecan 96-well plate reader. Samples were prepared in triplicate, averages and 1SD are shown. **C.** CLSM images of fluorescence, transmitted light, and their overlay are presented. At least three images were taken, and one representative example is shown. Laser intensity was 40 % unless specified otherwise, excitation wavelength was 550 nm and emission was 600 nm for all samples.*

A

401

B

402
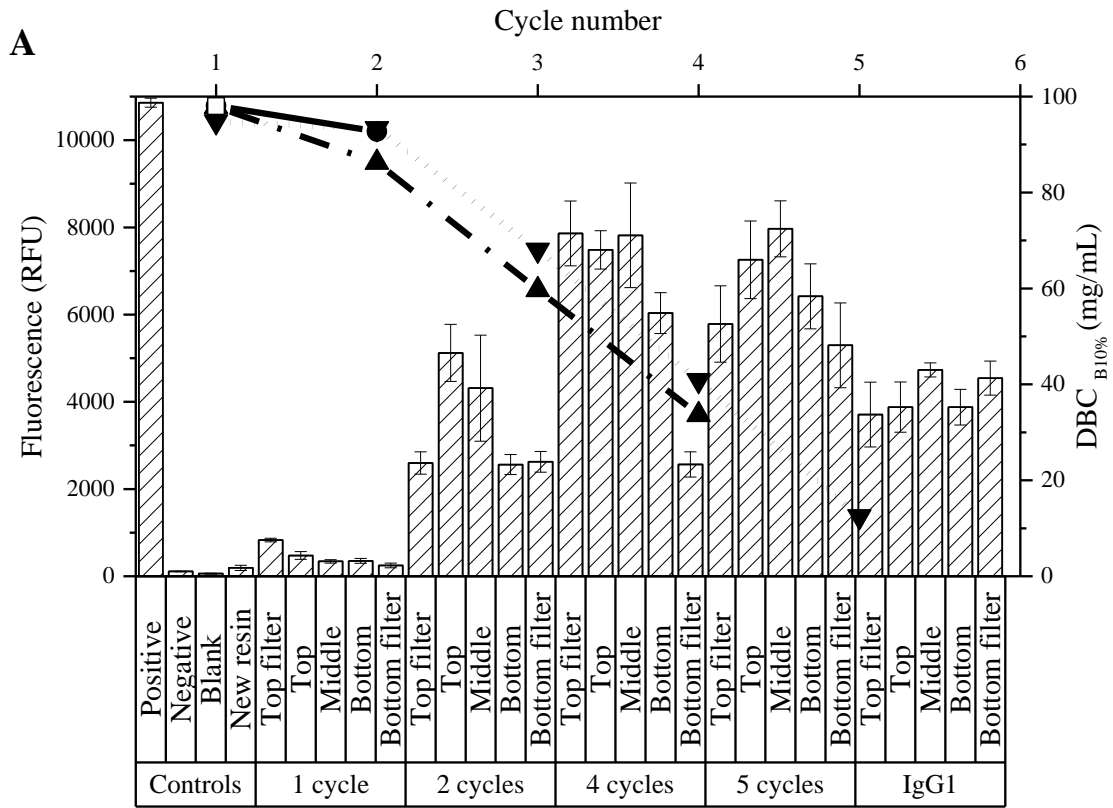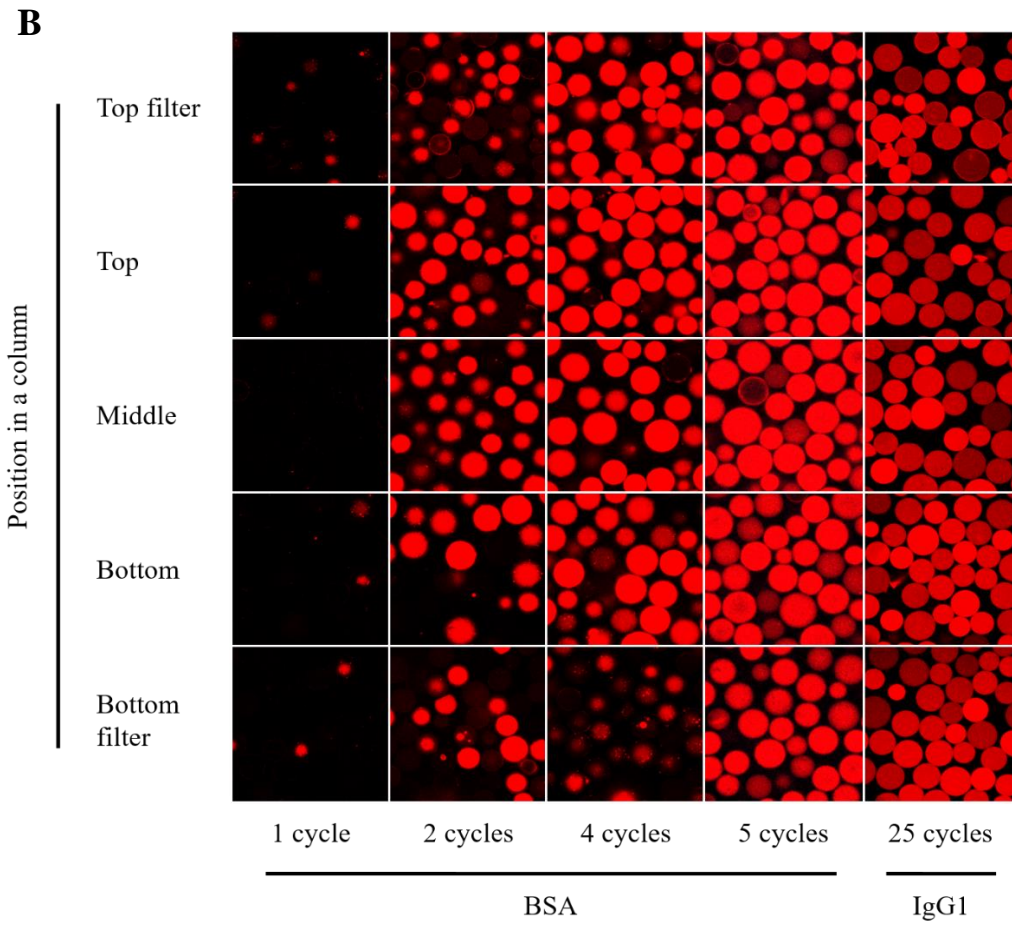
Figure 4. Fouling heterogeneity at column level. **A.** *Combined dynamic binding capacity and fluorescence intensity results. Dynamic binding capacity at 10 % breakthrough over cycle number is reflected as a line graph with measurements on the right y axis. DBC was performed with 200 mg of BSA per cycle for up to 5 cycles, and with 25 mg of IgG1 per cycle for 25 cycles at 50 cm/h flow rate. BSA cycles had a salt strip and a 1 M NaOH CIP step, whereas IgG1 cycles had only a 0.5 M NaCl strip step. After each number of cycles (i.e., 1, 2, 4 and 5) resin was separated into sections (i.e., top, middle, bottom), and stained with a dye followed by a fluorescence reading. Fluorescence intensity is shown as a column graph with measurements on the left y axis. Samples for fluorescence readings were prepared in triplicate, averages and 1SD are shown.* **B**. *CLSM images of fluorescence, transmitted light, and their overlay are presented. At least three images were taken of top filter (0.2 cm), top (1.5 cm), middle (1.5 cm), bottom (1.5 cm), and bottom filter (0.2 cm) part of the column, and one representative example image is shown. Laser intensity was 40 %, excitation wavelength was 550 nm and emission was 600 nm for all samples.*
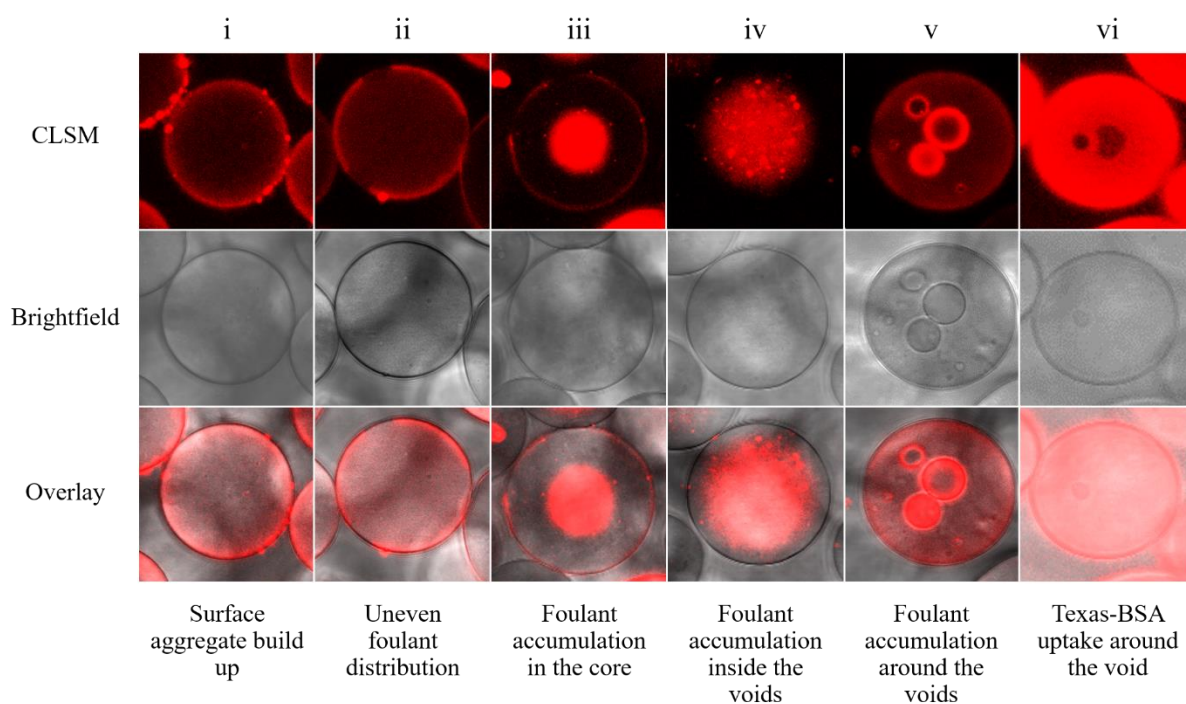
*Figure 5. Fouling heterogeneity at bead level. CLSM images of fluorescence, transmitted light, and their overlay are presented. At least three images were taken, and one representative is shown. Images (**i-v**) were generated using different cleaning conditions and taken from different locations in the column. Image (**vi**) was generated using Texas Red labelled BSA in a flow cell during a real-time loading step. Laser intensity was 40 %, excitation wavelength was 550 nm and emission was 600 nm for all samples.*

References:

[1]   M.C. Nweke, A.S. Rathore, D.G. Bracewell, Lifetime and Aging of Chromatography Resins during Biopharmaceutical Manufacture, Trends Biotechnol. (2018). doi:10.1016/j.tibtech.2018.01.001.

[2]   G. Sofer, J. Yourkin, Cleaning and cleaning validation in process chromatography. Current industry practices and future., BioProcess Tech. (2007) 72–82.

[3]   A. Grönberg, M. Eriksson, M. Ersoy, H.J. Johansson, A tool for increasing the lifetime of chromatography resins, MAbs. (2011). doi:10.4161/mabs.3.2.14874.

[4]   T. Elich, T. Iskra, W. Daniels, C.J. Morrison, High throughput determination of cleaning solutions to prevent the fouling of an anion exchange resin, Biotechnol. Bioeng. (2016). doi:10.1002/bit.25881.

[5]   A.S. Rathore, G. Sofer, Examples of scale down models, in: Process Valid. Manuf. Biopharm., Taylor & Francis Group, Boca Raton, 2005: pp. 75–82.

[6]   A.S. Rathore, G. Sofer, Experimental approaches to determine and validate chromatography media life span, in: Process Valid. Manuf. Biopharm., Taylor & Francis Group, Boca Raton, 2005: pp. 180–193.

[7]   L. Bousse, S. Mouradian, A. Minalla, H. Yee, K. Williams, R. Dubrow, Protein sizing on a microchip, Anal. Chem. (2001). doi:10.1021/ac0012492.

[8]   Y. Yigzaw, R. Piper, M. Tran, A.A. Shukla, Exploitation of the adsorptive properties of depth filters for host cell protein removal during monoclonal antibody purification, in: Biotechnol. Prog., 2006. doi:10.1021/bp050274w.

[9]   T. Iskra, G.R. Bolton, J.L. Coffman, R. Godavarti, The effect of protein a cycle number on the performance and lifetime of an anion exchange polishing step, Biotechnol. Bioeng. (2013). doi:10.1002/bit.24781.

[10]   P. Gagnon, R. Nian, J. Lee, L. Tan, S.M.A. Latiff, C.L. Lim, C. Chuah, X. Bi, Y. Yang, W. Zhang, H.T. Gan, Nonspecific interactions of chromatin with immunoglobulin G and protein A, and their impact on purification performance, J. Chromatogr. A. (2014). doi:10.1016/j.chroma.2014.03.010.

[11]   T. Bergander, K. Nilsson-Välimaa, K. Öberg, K.M. Lacki, High-throughput process development: Determination of dynamic binding capacity using microtiter filter plates filled with chromatography resin, in: Biotechnol. Prog., 2008. doi:10.1021/bp0704687.

[12]   M. Boulet-Audet, B. Byrne, S.G. Kazarian, Cleaning-in-place of immunoaffinity resins monitored by in situ ATR-FTIR spectroscopy, Anal. Bioanal. Chem. (2015). doi:10.1007/s00216-015-8871-3.

[13]   M. Boulet-Audet, S.G. Kazarian, B. Byrne, In-column ATR-FTIR spectroscopy to monitor affinity chromatography purification of monoclonal antibodies, Sci. Rep. (2016). doi:10.1038/srep30526.

[14]   J.M. Angelo, A. Cvetkovic, R. Gantier, A.M. Lenhoff, Characterization of cross-linked cellulosic ion-exchange adsorbents: 1. Structural properties, J. Chromatogr. A. (2013). doi:10.1016/j.chroma.2013.10.003.

[15]   J.M. Angelo, A. Cvetkovic, R. Gantier, A.M. Lenhoff, Characterization of cross-linked cellulosic ion-exchange adsorbents: 2. Protein sorption and transport, J. Chromatogr. A. (2016). doi:10.1016/j.chroma.2016.02.019.

467   [16]   E.J. Close, J.R. Salm, T. Iskra, E. Sørensen, D.G. Bracewell, Fouling of an anion exchange
468   chromatography operation in a monoclonal antibody process: Visualization and kinetic studies,
469   Biotechnol. Bioeng. 110 (2013) 2425–2435. doi:10.1002/bit.24898.

470   [17]   R. Corbett, G. Carta, T. Iskra, C. Gallo, R. Godavarti, J.R. Salm, Structure and protein
471   adsorption mechanisms of clean and fouled tentacle-type anion exchangers used in a
472   monoclonal antibody polishing step, J. Chromatogr. A. (2013).
473   doi:10.1016/j.chroma.2013.01.006.

474   [18]   S. Zhang, W. Daniels, J. Salm, J. Glynn, J. Martin, C. Gallo, R. Godavarti, G. Carta, Nature of
475   foulants and fouling mechanism in the Protein A MabSelect resin cycled in a monoclonal
476   antibody purification process, Biotechnol. Bioeng. (2016). doi:10.1002/bit.25706.

477   [19]   S. Zhang, K. Xu, W. Daniels, J. Salm, J. Glynn, J. Martin, C. Gallo, R. Godavarti, G. Carta,
478   Structural and functional characteristics of virgin and fouled Protein A MabSelect resin cycled
479   in a monoclonal antibody purification process, Biotechnol. Bioeng. (2016).
480   doi:10.1002/bit.25708.

481   [20]   M.C. Nweke, M. Turmaine, R.G. McCartney, D.G. Bracewell, Drying techniques for the
482   visualisation of agarose-based chromatography media by scanning electron microscopy,
483   Biotechnol. J. 12 (2017). doi:10.1002/biot.201600583.

484   [21]   S.C. Siu, R. Boushaba, V. Topoyassakul, A. Graham, S. Choudhury, G. Moss, N.J. Titchener-
485   Hooker, Visualising fouling of a chromatographic matrix using confocal scanning laser
486   microscopy, Biotechnol. Bioeng. 95 (2006) 714–723. doi:10.1002/bit.21028.

487   [22]   M. Pathak, K. Lintern, V. Chopda, D.G. Bracewell, A.S. Rathore, Fluorescence based real
488   time monitoring of fouling in process chromatography, Sci. Rep. (2017).
489   doi:10.1038/srep45640.

490   [23]   M. Pathak, A.S. Rathore, Implementation of a fluorescence based PAT control for fouling of
491   protein A chromatography resin, J. Chem. Technol. Biotechnol. (2017). doi:10.1002/jctb.5358.

492   [24]   D. Shen, J. Coleman, E. Chan, T.P. Nicholson, L. Dai, P.W. Sheppard, W.F. Patton, Novel
493   Cell- and Tissue-Based Assays for Detecting Misfolded and Aggregated Protein Accumulation
494   Within Aggresomes and Inclusion Bodies, Cell Biochem. Biophys. (2011).
495   doi:10.1007/s12013-010-9138-4.

496   [25]   R. Nelson, M.R. Sawaya, M. Balbirnie, A. Madsen, C. Riekel, R. Grothe, D. Eisenberg,
497   Structure of the cross-β spine of amyloid-like fibrils, Nature. (2005). doi:10.1038/nature03680.

498   [26]   N.K. Holm, S.K. Jespersen, L. V. Thomassen, T.Y. Wolff, P. Sehgal, L.A. Thomsen, G.
499   Christiansen, C.B. Andersen, A.D. Knudsen, D.E. Otzen, Aggregation and fibrillation of
500   bovine serum albumin, Biochim. Biophys. Acta - Proteins Proteomics. 1774 (2007) 1128–
501   1138. doi:10.1016/j.bbapap.2007.06.008.

502   [27]   V.A. Borzova, K.A. Markossian, N.A. Chebotareva, S.Y. Kleymenov, N.B. Poliansky, K.O.
503   Muranov, V.A. Stein-Margolina, V. V. Shubin, D.I. Markov, B.I. Kurganov, Kinetics of
504   thermal denaturation andaggregation of bovine serum albumin, PLoS One. (2016).
505   doi:10.1371/journal.pone.0153495.

506   [28]   J. Hubbuch, M.R. Kula, Confocal laser scanning microscopy as an analytical tool in
507   chromatographic research, Bioprocess Biosyst. Eng. 31 (2008) 241–259. doi:10.1007/s00449-
508   008-0197-5.

509   [29]   D.C. Carter, X.M. He, S.H. Munson, P.D. Twigg, K.M. Gernert, M.B. Broom, T.Y. Miller,
510   Three-dimensional structure of human serum albumin., Science. (1989).
511   doi:10.1126/science.2727704.

512   [30]   J. Wen, T. Arakawa, J.S. Philo, Size-exclusion chromatography with on-line light-scattering,

513 absorbance, and refractive index detectors for studying proteins and their interactions, Anal.
514 Biochem. (1996). doi:10.1006/abio.1996.0345.

515 [31] N.R. Rovnyagina, N.N. Sluchanko, T.N. Tikhonova, V. V. Fadeev, A.Y. Litskevich, A.A.
516 Maskevich, E.A. Shirshin, Binding of thioflavin T by albumins: An underestimated role of
517 protein oligomeric heterogeneity, Int. J. Biol. Macromol. (2018).
518 doi:10.1016/j.ijbiomac.2017.12.002.

519 [32] M. Groenning, M. Norrman, J.M. Flink, M. van de Weert, J.T. Bukrinsky, G. Schluckebier, S.
520 Frokjaer, Binding mode of Thioflavin T in insulin amyloid fibrils, J. Struct. Biol. (2007).
521 doi:10.1016/j.jsb.2007.06.004.

522 [33] M. Groenning, L. Olsen, M. van de Weert, J.M. Flink, S. Frokjaer, F.S. Jørgensen, Study on
523 the binding of Thioflavin T to β-sheet-rich and non-β-sheet cavities, J. Struct. Biol. (2007).
524 doi:10.1016/j.jsb.2006.12.010.

525 [34] P. Sen, S. Fatima, B. Ahmad, R.H. Khan, Interactions of thioflavin T with serum albumins:
526 Spectroscopic analyses, Spectrochim. Acta - Part A Mol. Biomol. Spectrosc. (2009).
527 doi:10.1016/j.saa.2009.05.010.

528 [35] S. Oshinbolu, R. Shah, G. Finka, M. Molloy, M. Uden, D.G. Bracewell, Evaluation of
529 fluorescent dyes to measure protein aggregation within mammalian cell culture supernatants, J.
530 Chem. Technol. Biotechnol. (2018). doi:10.1002/jctb.5519.

531 [36] A. Matlschweiger, P. Fuks, G. Carta, R. Hahn, Hindered diffusion of proteins in mixture
532 adsorption on porous anion exchangers and impact on flow-through purification of large
533 proteins, J. Chromatogr. A. (2019). doi:10.1016/j.chroma.2018.11.060.

534 [37] A.M. Gospodarek, D.E. Hiser, J.P. O'Connell, E.J. Fernandez, Unfolding of a model protein
535 on ion exchange and mixed mode chromatography surfaces, J. Chromatogr. A. (2014).
536 doi:10.1016/j.chroma.2014.06.024.

537 [38] R. Gillespie, T. Nguyen, S. Macneil, L. Jones, S. Crampton, S. Vunnum, Cation exchange
538 surface-mediated denaturation of an aglycosylated immunoglobulin (IgG1), J. Chromatogr. A.
539 (2012). doi:10.1016/j.chroma.2012.06.037.

540 [39] H. Luo, N. Macapagal, K. Newell, A. Man, A. Parupudi, Y. Li, Y. Li, Effects of salt-induced
541 reversible self-association on the elution behavior of a monoclonal antibody in cation
542 exchange chromatography, J. Chromatogr. A. (2014). doi:10.1016/j.chroma.2014.08.048.

543 [40] J. Guo, S. Zhang, G. Carta, Unfolding and aggregation of a glycosylated monoclonal antibody
544 on a cation exchange column. Part I. Chromatographic elution and batch adsorption behavior,
545 J. Chromatogr. A. (2014). doi:10.1016/j.chroma.2014.06.037.

546 [41] J. Guo, A.D. Creasy, G. Barker, G. Carta, Surface induced three-peak elution behavior of a
547 monoclonal antibody during cation exchange chromatography, J. Chromatogr. A. (2016).
548 doi:10.1016/j.chroma.2016.10.061.

549 [42] J. Guo, G. Carta, Unfolding and aggregation of a glycosylated monoclonal antibody on a
550 cation exchange column. Part II. Protein structure effects by hydrogen deuterium exchange
551 mass spectrometry, J. Chromatogr. A. (2014). doi:10.1016/j.chroma.2014.06.038.

552 [43] J. Guo, G. Carta, Unfolding and aggregation of monoclonal antibodies on cation exchange
553 columns: Effects of resin type, load buffer, and protein stability, J. Chromatogr. A. (2015).
554 doi:10.1016/j.chroma.2015.02.047.

555 [44] A.H. Clark, D.H.P. Saunderson, A. Suggett, Infrared and laser-raman spectroscopic studies of
556 thermally-induced globular protein gels, Int. J. Pept. Protein Res. (1981). doi:10.1111/j.1399-
557 3011.1981.tb02002.x.

558 [45] M. Pathak, A.S. Rathore, K. Lintern, D.G. Bracewell, Protein A chromatography resin
559   lifetime—impact of feed composition, Biotechnol. Prog. (2018). doi:10.1002/btpr.2608.

560 [46] S.C. Siu, R. Boushaba, J. Liau, R. Hjorth, N.J. Titchener-Hooker, Confocal imaging of
561   chromatographic fouling under flow conditions, J. Chem. Technol. Biotechnol. (2007).
562   doi:10.1002/jctb.1728.

563 [47] K. Lintern, M. Pathak, C.M. Smales, K. Howland, A. Rathore, D.G. Bracewell, Residual on
564   column host cell protein analysis during lifetime studies of protein A chromatography, J.
565   Chromatogr. A. 1461 (2016) 70–77. doi:10.1016/j.chroma.2016.07.055.

566 [48] M. Pathak, A.S. Rathore, Mechanistic understanding of fouling of protein A chromatography
567   resin, J. Chromatogr. A. 1459 (2016) 78–88. doi:10.1016/j.chroma.2016.06.084.

568 [49] J. Hubbuch, T. Linden, E. Knieps, J. Thömmes, M.R. Kula, Dynamics of protein uptake within
569   the adsorbent particle during packed bed chromatography, Biotechnol. Bioeng. 80 (2002) 359–
570   368. doi:10.1002/bit.10500.

571 [50] R. Hahn, R. Hahn, R. Schlegel, R. Schlegel, A. Jungbauer, A. Jungbauer, C omparison of
572   protein A affinity sorbents, J. Chromatogr. B. (2003). doi:10.1016/S1570-0232(03)00092-8.

573 [51] R. Hahn, P. Bauerhansl, K. Shimahara, C. Wizniewski, A. Tscheliessnig, A. Jungbauer,
574   Comparison of protein A affinity sorbents: II. Mass transfer properties, J. Chromatogr. A.
575   (2005). doi:10.1016/j.chroma.2005.07.050.

576 [52] T.F. Johnson, J.J. Bailey, F. Iacoviello, J.H. Welsh, P.R. Levison, P.R. Shearing, D.G.
577   Bracewell, Three dimensional characterisation of chromatography bead internal structure using
578   X-ray computed tomography and focused ion beam microscopy, J. Chromatogr. A. (2018).
579   doi:10.1016/j.chroma.2018.06.054.

580 [53] N. Garti, C. Bisperink, Double emulsions: Progress and applications, Curr. Opin. Colloid
581   Interface Sci. (1998). doi:10.1016/S1359-0294(98)80096-4.

582 [54] S. Okushima, T. Nisisako, T. Torii, T. Higuchi, Controlled production of monodisperse double
583   emulsions by two-step droplet breakup in microfluidic devices, Langmuir. (2004).
584   doi:10.1021/la0480336.

585 [55] T. Nisisako, S. Okushima, T. Torii, Controlled formulation of monodisperse double emulsions
586   in a multiple-phase microfluidic system, Soft Matter. (2005). doi:10.1039/b501972a.

587